Supporting Information

Functionalization of Metal Surface via Thiol-Ene Click Chemistry: Synthesis, Adsorption Behavior, and Post-Functionalization of a Catechol- and Allyl-Containing Copolymer

Yucheng Zhang,[1] Chien-Wei Chu,[1] Wei Ma,[1,2] and Atsushi Takahara[1,2]*

[1]Institute for Materials Chemistry and Engineering, Kyushu University, Nishi-ku, Fukuoka, 819-0395, Japan.

[2]International Institute for Carbon-Neutral Energy Research (WPI-I^{2}CNER), Kyushu University, Nishi-ku, Fukuoka, 819-0395, Japan.

KEYWORDS: epoxy adhesives, catechol anchoring, surface modification, metallic material

1. Synthesis of P(MEUE-*co*-DOPAm)

The signals of allylic double bonds appeared at similar chemical shifts (~5.81 and ~4.97 ppm) to those in MEUE monomer, indicating the existence of the clickable agents in the copolymer. Meanwhile, the molar ratio between $DOPAm_{TBDMS}$ (M1) and MEUE (M2) segments was estimated by the following equation:

$$\frac{M1}{M2} = (I_{6.56-6.89}/3) : (I_{4.98}/2) \quad \text{(S1)}$$

where the $I_{4.98}$ is the integration of the signal at 4.98 ppm, corresponding to 2 hydrogen atoms in an allyl group; the $I_{6.56\text{-}6.89}$ is the integration of the signals from 6.56 to 6.89 ppm, assigned to 3 hydrogen atoms in a catechol group. The calculated $\frac{M1}{M2}$ is 1:2.7, which is slightly lower than the feed ratio (1:3).

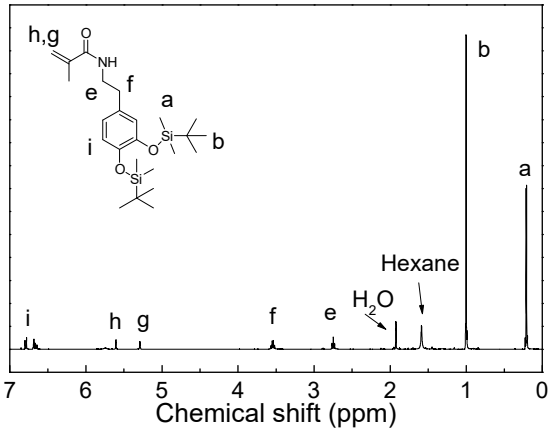

Figure S1. ^{1}H NMR spectrum of $DOPAm_{TBDMS}$.

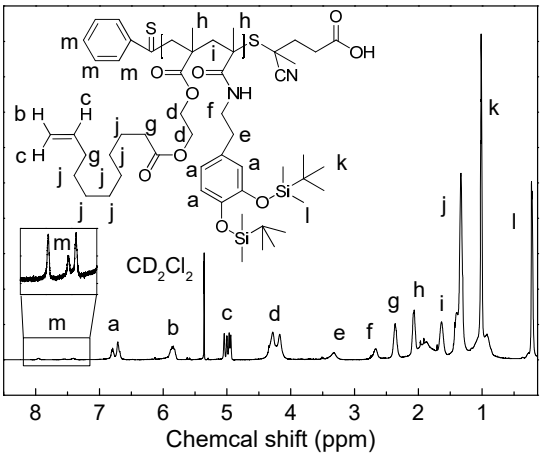

Figure S2. ^{1}H NMR spectrum of P(MEUE-*co*-DOPAm$_{TBDMS}$).

Table S1. Information of allyl-containing copolymer

Polymer	Feed ratio [a]	M_n' [b]	M_n [c]	M_w [c]	PDI [c]
P(AMA-co-DOPAm$_{TBDMS}$)	3:1	10,000	26,300	81,500	3.1
P(MEUE-co-DOPAm$_{TBDMS}$)	3:1	10,000	14,400	22,600	1.5

[a]Molar feed ratio between AMA/MEUE and DOPAm$_{TBDMS}$; [b]M_n' is the designed molecular weight; [b]M_n, M_w, and PDI were obtained from SEC measurements using DMF as the elution.

2. Click reaction of P(MEUE-*co*-DOPAm$_{TBDMS}$)

The post-functionalization of P(MEUE-*co*-DOPAm$_{TBDMS}$) *via* the thiol-ene click chemistry was demonstrated using 1-dodecanethiol and Irgacure 2959 as the template thiol and the photo-initiator, respectively. After the photo-initiators were irradiated by UV lights, photo-radicals can be generated to mediate the thiol-ene click reactions. Nevertheless, it is also possible that the photo-radicals may trigger the side reactions on allyl-containing copolymer itself, such as cross-linking. To verify the potential side reactions, the P(MEUE-*co*-DOPAm$_{TBDMS}$) (20 mg, 1.4 nmol) was mixed with Irgacure 2959 (0.2 mg) and 1-dodecanethiol (14 mg, 70 nmol) in chloroform (0.4 mL),

followed by a UV irradiation (0.9 mW/cm^2 at 256 nm) for 20 min at 298K. After the click reaction, the resultant polymer was purified by precipitation in methanol for 3 times. For comparison purposes, another click reaction without adding 1-dodecanethiol was also carried out under similar conditions.

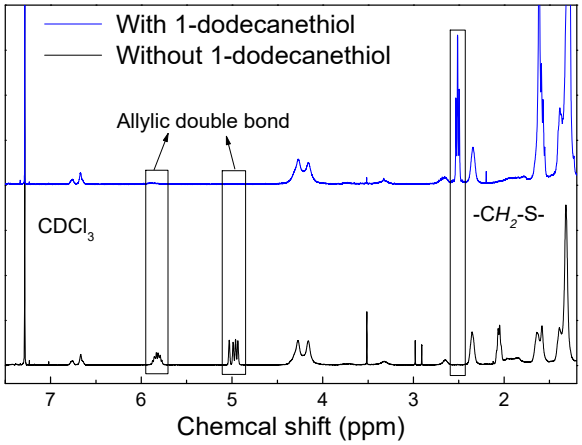

Figure S3. ^{1}H NMR spectra of P(MEUE-co-DOPAm$_{TBDMS}$) after 20 min UV irradiation with or without 1-dodecanethiol.

The color changes after the UV irradiations and the ^{1}H NMR data (Figure S3) were used to evaluate the side reactions of the thiol-ene click reactions. For the sample without 1-dodecanethiol, the pink solution was turned into colorless after the UV irradiation. As the ratio between the signals of the catechol units and allylic double bonds in the ^{1}H NMR spectrum (Figure S3, black curve) is constant, neither the thiol-ene click reaction nor the other side reactions on allyl group took place. The color change may be only caused by the oxidation of the RAFT agent in copolymer because the similar changes were observed in the literature, discussing the coexistence of the dithioates and radicals in an open-air. For the sample with 1-dodecanethiol, the color change was also observed. Furthermore, the absence of the peaks at ~4.98 ppm (the allylic double bonds) and the presence of a new peak at ~2.52 ppm (the hydrogens in two methylene groups adjacent to the sulfur atom)

appeared in the ^{1}H NMR spectrum (Figure S3, blue curve), indicating the successful functionalization of P(MEUE-*co*-DOPAm$_{TBDMS}$). Since the signals of the allylic double bond are extremely weak, the click reaction under this condition has a very high conversion rate, which is well applicable for surface functionalization.

3. Adsorption behavior of P(MEUE-*co*-DOPAm)

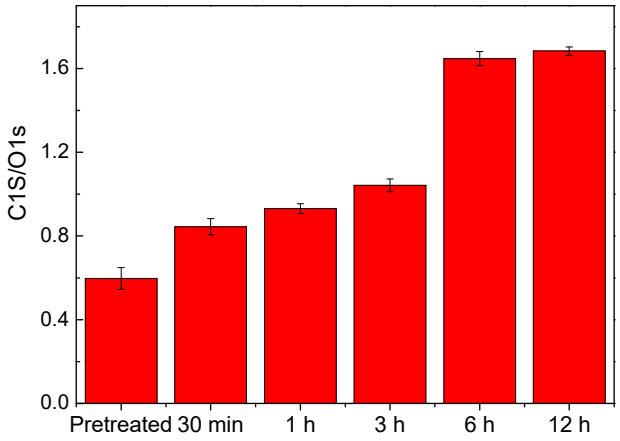

Figure S4. C_{1s}/O_{1s} changes of SUS-*g*-P(MEUE-*co*-DOPAm) with various immersion durations.

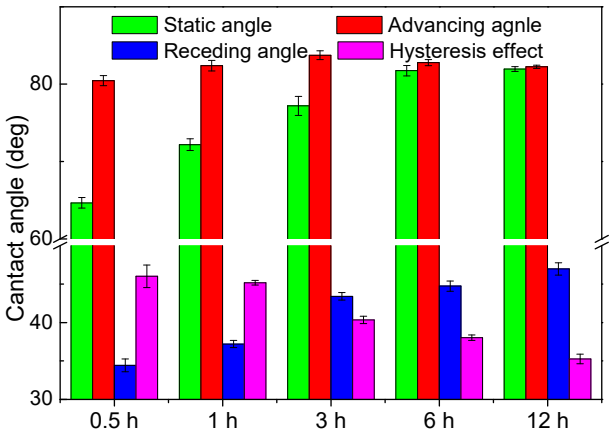

Figure S5. Contact angle changes of SUS-*g*-P(MEUE-*co*-DOPAm) with various immersion durations.

To give the adsorption behavior of P(MEUE-*co*-DOPAm), the sample with different immersion time (30 min, 1 h, 3 h, 6 h, and 12 h) were prepared, and the XPS and contact angle measurements were performed. The atomic ratio between carbon and oxygen atoms (C/O) was calculated from the high-resolution scan of C_{1s} and O_{1s} to show the film formation. As shown in Figure S4, The C/O increased with the increase of immersion time and reached the maximum after 6 h. This result indicates the coating formation was enhanced by the immersion duration and reach saturation adsorption after 6 h immersion.

Figure S5 shows the static and dynamic contact angle, as well as the contact angle hysteresis of the samples. The static contact angle increased from 10 min to 6 h. This tendency is in accordance with the XPS results, implying the saturation was achieved at 6 h. As for the dynamic contact angle, despite the fact that the sample with different durations showed a similar advancing angle, the receding angle gradually increased from 34.4° to 47.0°, and the contact angle hysteresis decreased from 46.0° to 35.3°.

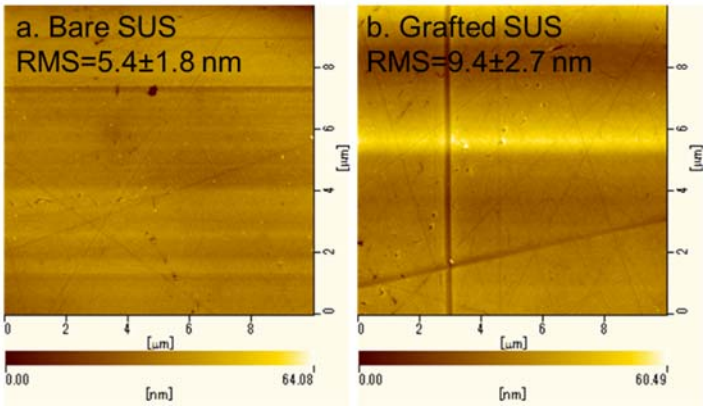

Figure S6. AFM images of SUS substrate before (a) and after (b) polymer adsorption.

4. Surface functionalization using hydrophobic thiol

4.1. Optimization of UV conditions

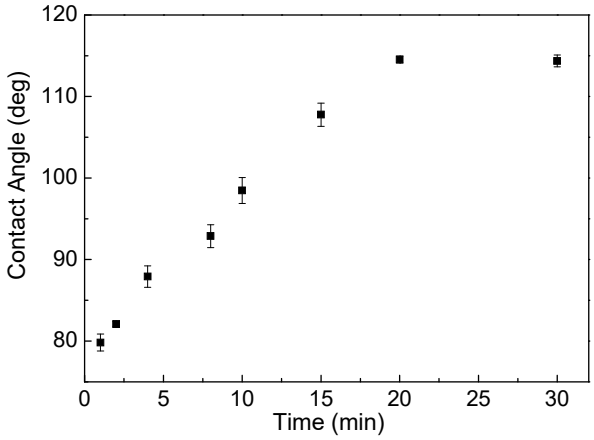

Figure S7. Contact angle of SUS-*g*-P(MEUE-*co*-DOPAm) after click reaction with various reaction durations.

The change of surface wettabilities with various durations of UV irradiation was investigated by the static contact angle measurements using 2 μL water droplets as a probe liquid. The increasing tendency of contact angles was elevated in Figure S6, indicating the progress of PFDT grafting. The maximum contact angles of ~110° were obtained in the SUS samples with 20 min irradiation, suggesting that the equilibrium states for the click reactions were achieved. It is worth to note that longer exposure times over 30 min might induce the oxidation of the thiol groups; thus the optimum exposure times were between 20-30 min.

4.2. Surface functionalization on various metals

For the PFDT functionalization of various metals, the signals of F_{1s} were observed in the spectrum of survey scan (Figure S7) on all kinds of metal surface; the C/O ratios were increased to 1.60 (Al), 2.13 (Ni), and 1.76 (Ti) after surface modification (Table S3). The two peaks related

to CF_2 and CF_3 appeared in the high-resolution spectra of C_{1s}. The contact angle of the PFDT-modified surface is higher than 107° after the modification (Table S3).

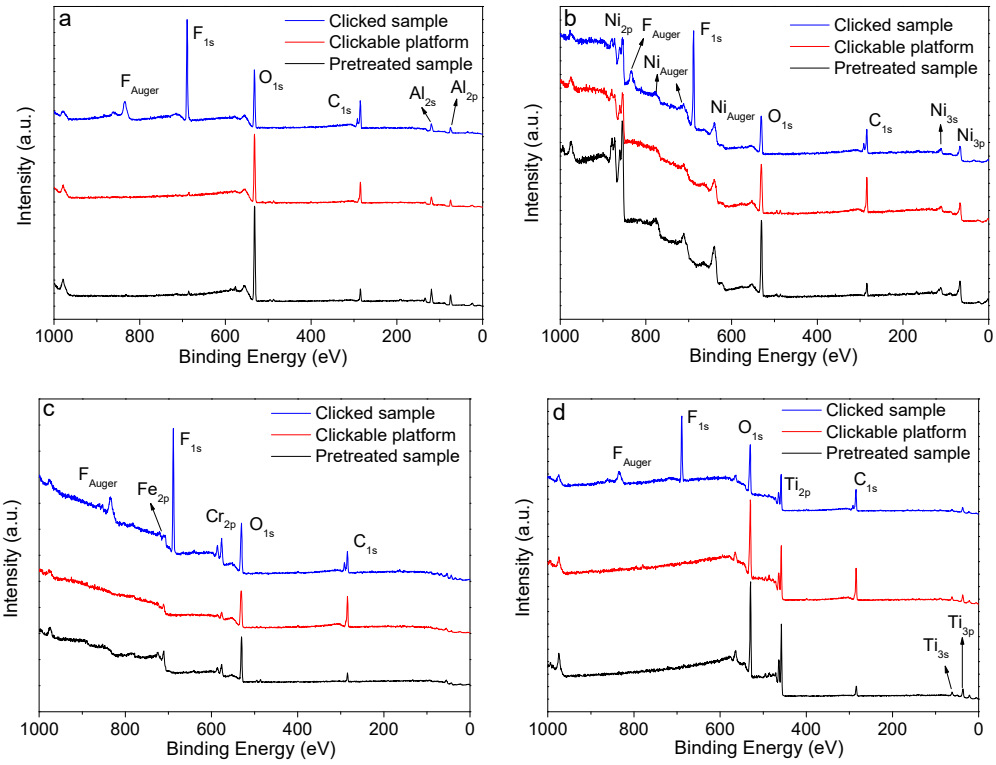

Figure S8. Survey scan of the metal substrates after the clean procedure (black line), polymer adsorption (red line), and PFDT functionalization (blue line), (a) Al, (b) Ni, (c) SUS, and (d) Ti.

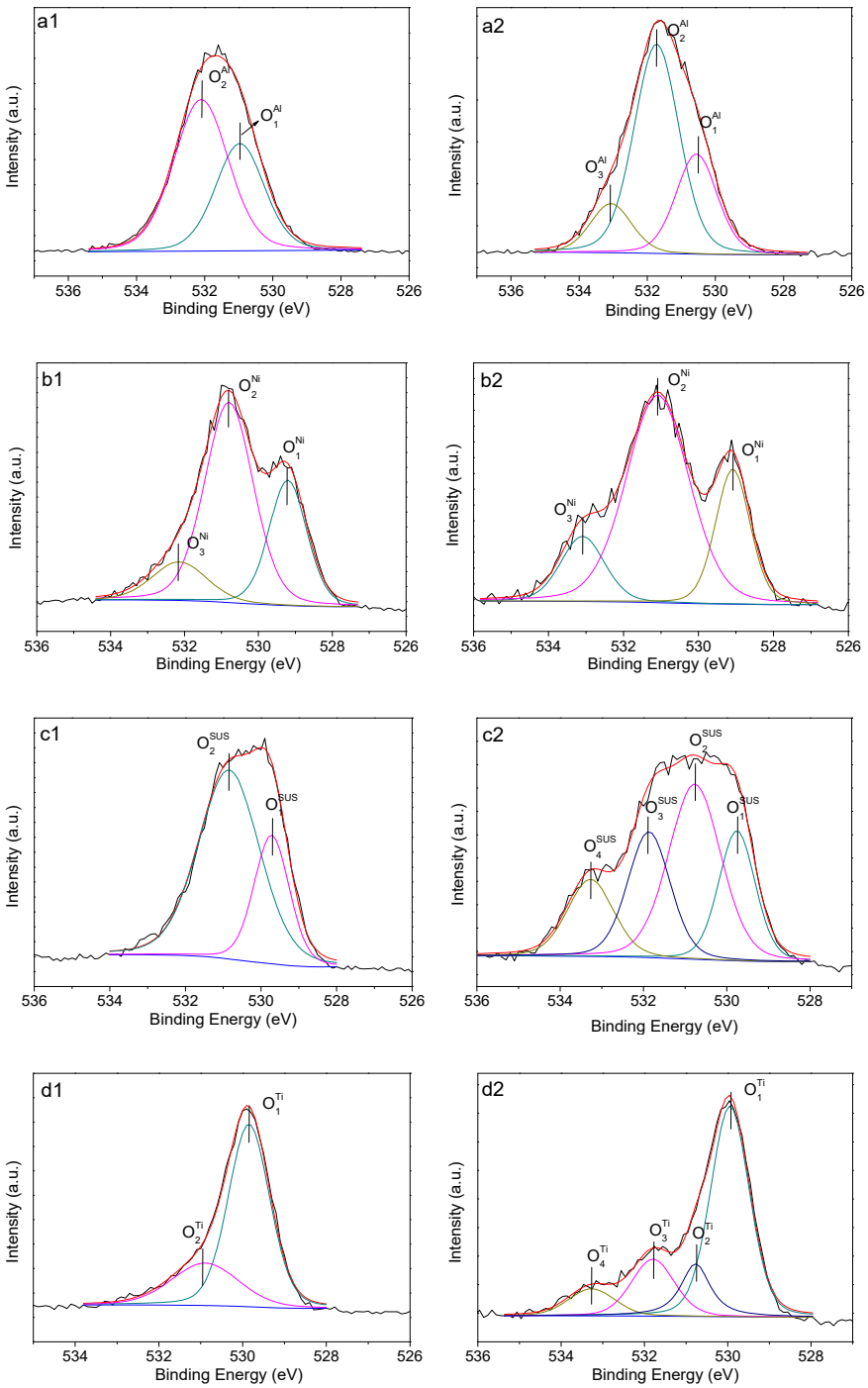

Figure S9. High-resolution spectra of O1s for (a) Al, (b) Ni, (c) SUS, and (d) Ti (1) before and (2) after P(MEUE-*co*-DOPAm) adsorption.

Table S2. Fitting information of O1s high-resolution scan

Sample		Label	Proposed components	Binding energy (eV)	FWHM (eV)
Pretreated	Al	O_1^{Al}	Al-O	530.8	1.68
		O_2^{Al}	Al-OH	531.9	1.89
	Ni	O_1^{Ni}	Ni-O	529.2	1.13
		O_2^{Ni}	Ni-OH	531.0	1.77
		O_3^{Ni}	Ni-OO	532.5	1.60
	SUS	O_1^{SUS}	Fe-O/Cr-O	529.7	1.10
		O_2^{SUS}	Fe-OH/Cr-OH	530.8	1.90
	`Ti	O_1^{Ti}	Al-O	529.9	1.18
		O_2^{Ti}	Al-OH	531.0	1.97
Clickable platform	Al	O_1^{Al}	Al-O	530.8	1.50
		O_2^{Al}	C-O	531.9	1.56
		O_3^{Al}	C=O	533.2	1.41
	Ni	O_1^{Ni}	Ni-O	529.2	1.05
		O_2^{Ni}	Ni-OH/C-O	531.3	2.10
		O_3^{Ni}	C=O	533.3	1.34
	SUS	O_1^{SUS}	Al-O	529.7	1.03
		O_2^{SUS}	Al-OH	530.7	1.47
		O_3^{SUS}	C-O	531.8	1.20
		O_4^{SUS}	C=O	533.2	1.30
	Ti	O_1^{Ti}	Al-O	530.0	1.10
		O_2^{Ti}	Al-OH	530.8	0.83
		O_3^{Ti}	C-O	531.8	1.21
		O_4^{Ti}	C=O	533.3	1.30

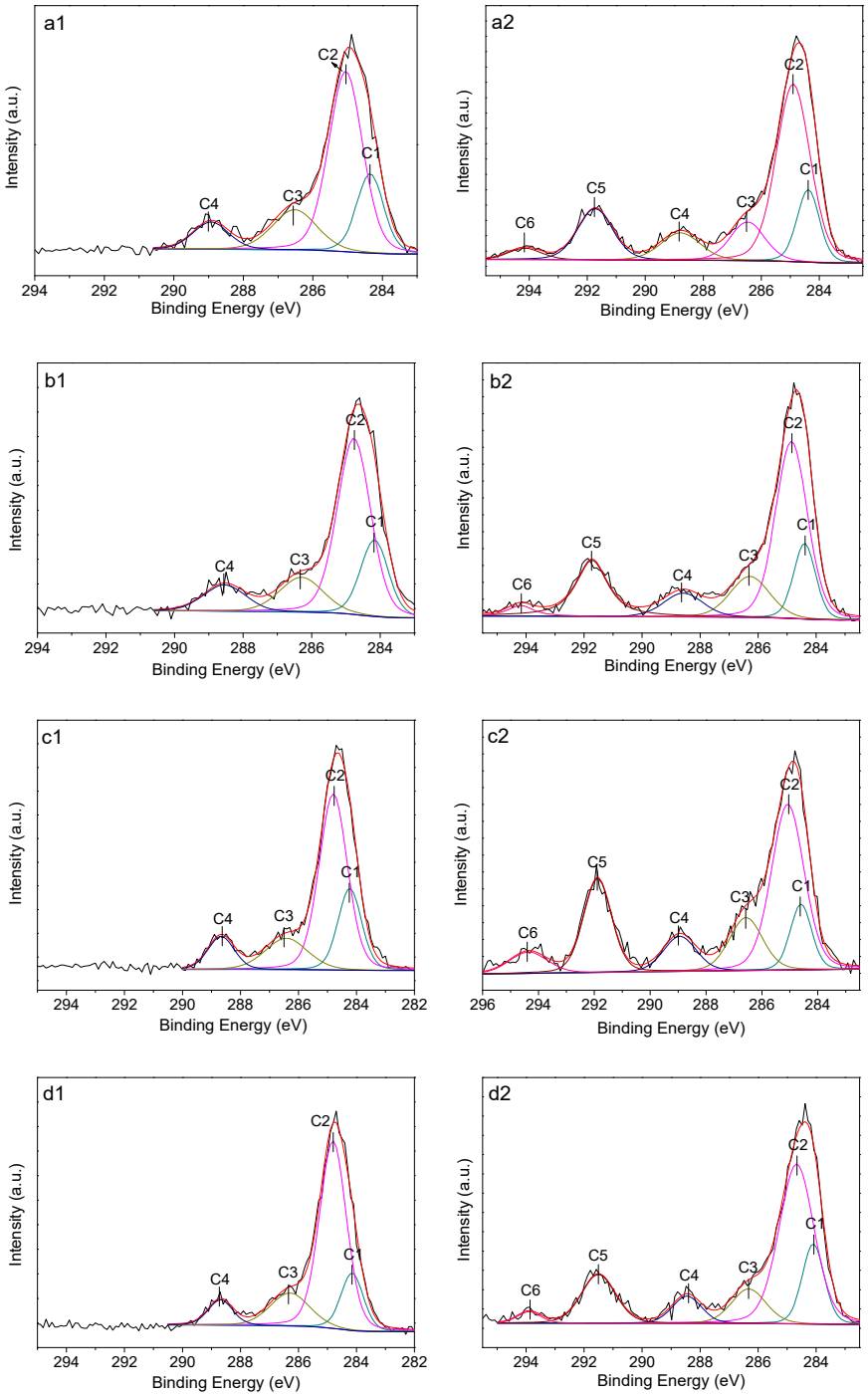

Figure S10. High-resolution spectra of C1s for (a) Al-*g*-P(MEUE-*co*-DOPAm), (b) Ni-*g*-P(MEUE-*co*-DOPAm), (c) SUS-*g*-P(MEUE-*co*-DOPAm), and (d) Ti-*g*-P(MEUE-*co*-DOPAm) (1) before and (2) after PFDT click reaction.

Table S3. Fitting information of C1s high-resolution scan

Sample		Label	Proposed components	Binding energy (eV)	FWHM (eV)
Clickable platform	Al	C1	Aromatic	284.4	0.91
		C2	C-C/C=C	285.1	1.16
		C3	C-O/C-N	287.0	1.47
		C4	COO/CON	289.4	1.27
	Ni	C1	Aromatic	284.4	0.95
		C2	C-C/C=C	285.0	1.20
		C3	C-O/C-N	286.6	1.53
		C4	COO/CON	288.8	1.29
	SUS	C1	Aromatic	284.4	0.96
		C2	C-C/C=C	285.0	1.15
		C3	C-O/C-N	286.5	1.75
		C4	COO/CON	288.8	1.03
	`Ti	C1	Aromatic	284.4	0.91
		C2	C-C/C=C	285.0	1.14
		C3	C-O/C-N	286.6	1.53
		C4	COO/CON	288.9	1.07
Clicked sample	Al	C1	Aromatic	284.4	0.92
		C2	C-C	284.9	1.36
		C3	C-O/C-N/C-S	286.3	1.40
		C4	COO/CON	288.7	1.58
		C5	CF2	291.7	1.32
		C6	CF3	294.1	1.17
	Ni	C1	Aromatic	284.4	0.90
		C2	C-C	284.8	1.32

	C3	C-O/C-N/C-S	286.2	1.52
	C4	COO/CON	288.5	1.65
	C5	CF2	291.7	1.27
	C6	CF3	294.1	1.22
SUS	C1	Aromatic	284.4	0.91
	C2	C-C	284.9	1.33
	C3	C-O/C-N/C-S	286.3	1.40
	C4	COO/CON	288.7	1.64
	C5	CF2	291.7	1.23
	C6	CF3	294.1	1.22
Ti	C1	Aromatic	284.4	0.90
	C2	C-C	285.0	1.30
	C3	C-O/C-N/C-S	286.3	1.60
	C4	COO/CON	288.7	1.11
	C5	CF2	291.8	1.27
	C6	CF3	294.2	0.91

Table S4. Contact angle data and C/O ratio of Al, Ni, SUS, and Ti in all samples

Sample	C/O[a]	θ_S (°)[b]
Pretreated Al	0.24±0.029	5.3±0.3
Pretreated Ni	0.43±0.023	6.7±0.3
Pretreated SUS	0.60 ±0.052	6.6±0.2
Pretreated Ti	0.38±0.0067	7.8±0.3
Al-*g*-P(MEUE-*co*-DOPAm)	0.93±0.03	83.0±0.7
Ni-*g*-P(MEUE-*co*-DOPAm)	1.81±0.07	77.9±0.5
SUS-*g*-P(MEUE-*co*-DOPAm)	1.68±0.01	83.7±1.3
Ti-*g*-P(MEUE-*co*-DOPAm)	1.28±0.05	81.7±0.6
PFDT-clicked Al	1.60±0.03	112.7±0.5
PFDT-clicked Ni	2.13±0.04	107.4±1.0
PFDT-clicked SUS	1.81±0.09	112.4±0.7
PFDT-clicked Ti	1.76±0.06	110.3±0.6

[a]Value of C/O ratio was calculated from the high-resolution scan of the C_{1s} and O_{1s} with three independent measurements. [b]Static contact angle was measured by 2 μL water droplet with five independent measurements.

4.3. Surface functionalization using MESNa

The surface wettabilities of hydrophilic functionalization were studied by the contact angle data, as summarized in Table S4. The water droplet in the air contact angle of the MESNa-clicked surfaces (~78.2°) was just slightly lower than that of the SUS-*g*-P(MEUE-*co*-DOPAm) (~83.7°) and much higher than the reported value (~18.0°) of a MESNa self-assembled monolayer on gold

surface. In dynamic water contact angle measurement, the receding angle reduced to ~20.5°, while the advancing angle slightly increased to ~89.8° after the click reaction. Even though the successful formation of the MESNa was confirmed by XPS data, it was inconsistent that there was no apparent change in wettabilities. This inconsistency could be explained by the surface reorganization during the solvent evaporation. The larger contact angle hysteresis of the surface after the click reaction (~70.1°) than that before the click reaction (35.8°) indirectly showed a higher surface inhomogeneity caused by the surface reorganization of MESNa molecules. To avoid the reorganization issue, the air bubble in water contact angle measurements were further carried out as described elsewhere. The air bubble in water contact angles of the clicked samples was ~38.3° larger than that before the click reaction, indicating the formation of a hydrophilic MESNa layer.

Table S5. Contact angle measurement for polymer and MESNa-modified SUS.

Sample	Water droplet (deg)[a]	Advancing angle (deg)[b]	Receding angle (deg)[b]	Air bubble (deg)[c]
SUS-*g*-P(MEUE-*co*-DOPAm)	83.7±1.3	89.8±0.4	54.0±1.6	109.8±2.2
SUS-*g*-MESNa	78.2±0.5	92.6±0.7	20.5±2.0	148.1±2.3

[a]Water droplet contact angle was performed using 2 μL water droplet; [b]The dynamic contact angle was evaluated on the basis of dynamic sessile drop method; [c]The air bubble contact angle was carried in water using 2 μL air bubble as a probe.

5. Functionalization of AAO

The theoretical contact angles of AAO-*g*-P(MEUE-*co*-DOPAm) and AAO-*g*-PFDT could be calculated using the following Cassie-Baxter equation:

$$\cos\theta_c = f(1+\cos\theta)-1 \quad \text{(S2)}$$

where the θ_c and θ are the contact angles on the textured surface (e.g. AAO membrane) and the flat surface (e.g. Al substrate), respectively; the f represents the fraction of the solid surface (i.e. AAO surface) in entire composite surface (ie. both AAO and air surfaces) beneath the water. The f was obtained from the area ratio between the AAO region and the pore region in the scanning electron microscope (SEM) images (the SEM images in the catalog of Whatman membrane filters was utilized). The surface fraction of the alumina phase was calculated using Image-J, which is 0.496.